Manuscript submitted to
AIMS' Journals
Volume **X**, Number **0X**, XX **200X**

doi:10.3934/xx.xx.xx.xx

pp. **X–XX**

# DESIGNING RENDEZVOUS MISSIONS WITH MINI-MOONS USING GEOMETRIC OPTIMAL CONTROL

Monique Chyba, Geoff Patterson and Gautier Picot

Department of Mathematics
University of Hawaii at Manoa
Honolulu, USA

Mikael Granvik

Department of Physics
University of Helsinki
Helsinki, Finland

Robert Jedicke

Institute for Astronomy
University of Hawaii at Manoa
Honolulu, USA

Jeremie Vaubaillon

Institut de Mécanique Céleste et de Calcul des Éphémérides
Observatoire de Paris
Paris, France

Abstract. Temporarily-captured Natural Earth Satellites (NES) are very appealing targets for space missions for many reasons. Indeed, NES get captured by the Earth's gravity for some period of time, making for a more cost-effective and time-effective mission compared to a deep-space mission, such as the 7-year Hayabusa mission. Moreover, their small size introduces the possibility of returning with the entire temporarily-captured orbiter (TCO) to Earth. Additionally, NES can be seen as interesting targets when examining figures of their orbits. It requires to expand the current state-of-art of the techniques in geometric optimal control applied to low-thrust orbital transfers. Based on a catalogue of over sixteen-thousand NES, and assuming ionic propulsion for the spacecraft, we compute time minimal rendezvous missions for more than 96% of the NES. The time optimal control transfers are calculated using classical indirect methods of optimal control based on the Pontryagin Maximum Principle. Additionally we verify the local optimality of the transfers using second order conditions.

2010 *Mathematics Subject Classification.* Primary: 49M05, 70M20; Secondary: 49K15.

*Key words and phrases.* Control theory, orbital transfer, natural Earth satellites, temporarily captured orbiters.

The reviewing process of the paper was handled by Ryan Loxton and Qun Lin as Guest Editors.

1. **Introduction.** Our era is witnessing an expansion in the complexity of endeavors beyond the Earth's orbit. Designing and executing space missions to reach asteroids in the universe has attracted much research over the past few decades. Near Earth asteroid rendezvous (NEAR) and Hayabusa (formerly known as MUSES-C) are completed missions that involved a rendezvous with an asteroid including a safe landing. Both missions took several years to complete with Eros and Itokawa, the respective asteroids for the NEAR and Hayabusa missions, being Mars-Crosser asteroids. The existence of temporarily-captured natural Earth satellites would literally provide a gateway for a breakthrough into our understanding of the universe. Indeed, temporarily-captured natural Earth satellites are close to Earth and revolve around it, and they are also small in size. This creates the opportunity for short time duration missions and therefore minimizes the cost. In their work [23], the authors construct a theoretical database of temporarily-captured natural Earth satellites. From this work, it can be observed that temporarily-captured natural Earth satellites presents a large variety of orbits from very regular to extremely scattered. This diversity of orbits is appealing because we can not only test the capabilities of our transfer computation methods, but also develop experience designing transfer maneuvers that may not have been completed before. Space missions to reach asteroids, comets or temporarily-captured natural Earth satellites present major challenges for the spacecraft. There is a need for techniques to produce years of orbit adjustment for the spacecraft to match position and velocity with these objects of negligible mass.

Rendezvous missions to temporarily-captured natural Earth satellites differ from NEAR and Hayabusa in several ways. Indeed, temporarily-captured natural Earth satellites are called irregular satellites. After their capture, they orbit the Earth for a finite time (that typically amounts to a few months) to eventually escape from Earth's gravity. As a consequence, tight time constraints become a major criterion when designing a mission to reach a temporarily-captured natural Earth satellite. The maximum propulsion allowed during an orbital transfer may vary highly, depending on the thrusters with which the spacecraft is equipped. This remains true even for long-duration (several-year) missions. As an example, a bipropellant 450N main thruster was used during the Near mission [35] whereas the main propulsion for the Hayabusa mission was provided by four ion thrusters, each of them supplying a maximum thrust of 4.8e-3N [25, 26]. It is consequently of high importance, to meet the engineering needs, to model transfers within a wide range of maximal thrusts. We consider in this paper a spacecraft equipped with a ion propulsion system, the lowest admissible thrust for our transfers to temporarily-captured natural Earth satellites is fixed 0.1N and the highest admissible thrust to be 1N. We first establish rendezvous missions for the highest thrust available, and then, for a sample of those temporarily-captured natural Earth satellites that can be reached with the maximum thrust, we use a continuation method to determine what is the lowest admissible thrust for a rendezvous mission to that temporarily-captured natural Earth satellite. Our study suggests that the minimum thrust that can be used is related to the velocities of the temporarily-captured natural Earth satellites at the rendezvous point.

The main goal of this paper is to apply techniques from geometric optimal control to determine the percentage of temporarily-captured natural Earth satellites to which we can design a rendezvous mission from the catalogue of the over sixteen-thousand ones computed in [23].

The outline of the paper is as follows. In section 2 we define temporarily-captured natural Earth satellites and introduce the database our work is based on. Section 3 is devoted to orbital transfers in general and the specific techniques of geometric optimal control. In section 4 we apply the tools introduced in section 3 to our problem and present our methodology to design the rendezvous missions. Finally, section 5 presents our results complemented by graphical representations.

2. **Temporarily-Captured Natural Earth Satellite.** Definition and detailed information about temporarily-captured natural Earth satellites can be found in [23]. We here only repeat the necessary background for the work presented in this paper.

In Granvik et. al. (2012) [23], the authors evaluate a population statistic for temporarily-captured natural Earth satellites, or so-called mini-moons. The work is based on an integration of 10 million "test-particles" in space to determine which do get temporarily captured by Earth's gravitational field. The authors obtained a catalogue of over eighteen-thousand meteoroids that would get temporarily captured. Our work is based on this characterization. We here actually consider 16,923 meteoroids from their catalogue for purely structural reasons (the files were not readable by us). The remaining ones will be treated in future work. It is from their integrated temporarily-captured natural Earth satellites database that we select our orbital transfer targets. Moreover, it can be shown statistically that there is at least one 1-m-diameter temporarily-captured natural Earth satellite orbiting the Earth at any given time.

Let us first introduce some precise definitions. A *natural Earth satellite*, or *NES*, is defined as a celestial body that orbits the Earth. More precisely, a natural object in space is defined as *temporarily-captured* by a planet (or any body orbiting the Sun, including the Moon) by requiring simultaneously, see [23], that

1. the planetocentric Keplerian energy $E_{planet} < 0$,
2. the planetocentric distance is less than three Hill radii for the planet in question (e.g., for the Earth $3R_{H,\oplus} \sim 0.03$ AU).

In addition, for an object to be considered a temporarily-captured *orbiter*, or *TCO*, we require that it makes at least one full revolution around the planet in a co-rotating frame while being captured (the line from the planet to the Sun is fixed in this coordinate system) [23] . As a convention for this paper, we will always be referring to TCO which orbit the Earth (though the definition is stated more generally), and so, in this paper, TCO will be equivalent to temporarily-captured NES.

Figure 1 presents five distinct TCO orbits. It can be observed that TCO's orbits can differ significantly in total amount of captured time and number of revolutions around the Earth.

Work is undergoing to design methodologies to detect TCOs. It presents many challenges, one of them being the small size of those objects. In the event that detection is successful, a well-defined algorithm to produce a space mission to rendezvous with the detected TCO is highly desirable to take advantage of this opportunity. This is the main focus of our work. The average number of revolutions around the Earth for a TCO is $2.88 \pm 0.82$, and the average time of capture $286 \pm 18$ days [23]. This makes those objects appealing targets. Indeed, an object in orbit provides more time for the detection, planning, and execution of a space mission, when compared to that of an object which just flies by, (i.e. does not orbit). The first step

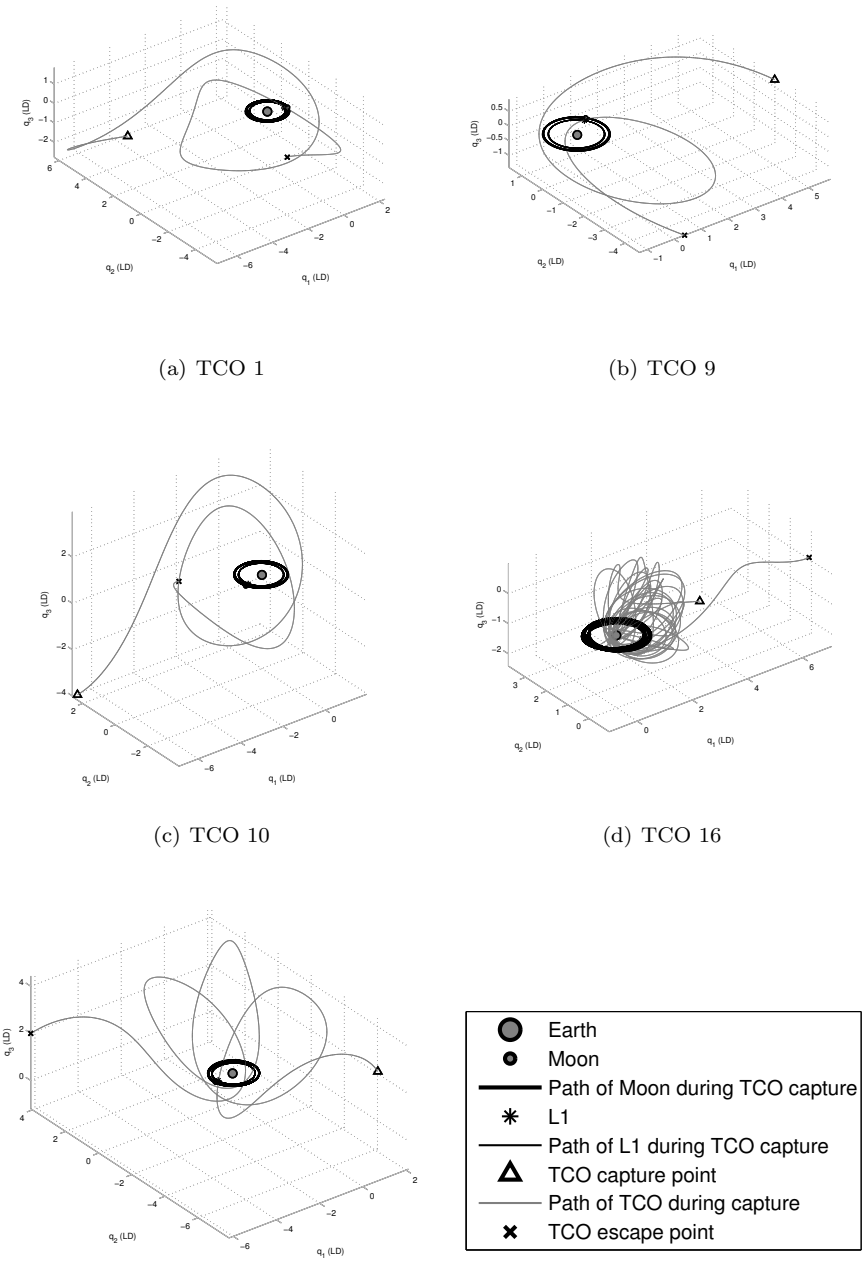


(a) TCO 1 (b) TCO 9

(c) TCO 10 (d) TCO 16

(e) TCO 19 (f) Legend

FIGURE 1. Examples of five TCO orbits with a variety of regularity, viewed in the inertial frame. A legend for all five plots is given in (f). The trajectories of the Moon and the theoretical point $L1$ are shown as the outer and inner rings (respectively) around Earth.

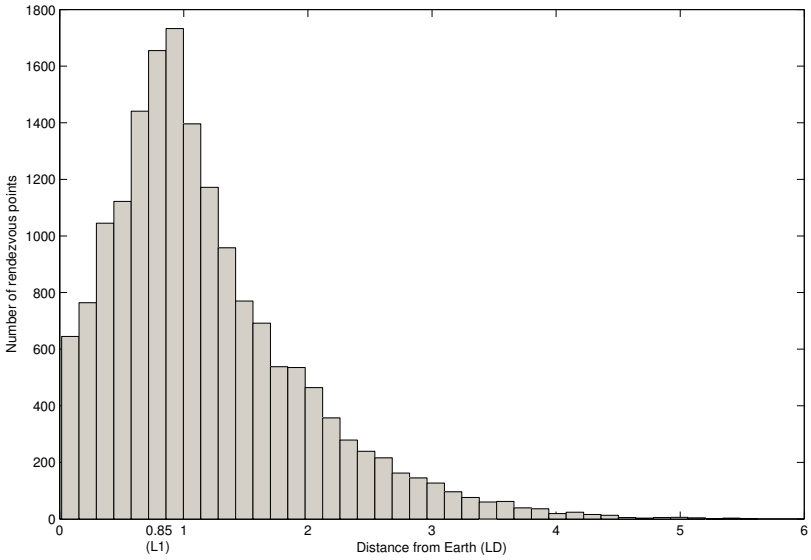


FIGURE 2. A histogram representing the distribution of rendezvous points with respect to their distance from Earth, where 1 Lunar distance (LD) = 384,400 km.

to a complete space mission to a TCO is to design a *rendezvous* with the TCO, by which we mean that the spacecraft must match the position and velocity of the TCO at the selected point.

Clearly, a critical aspect in the design of a rendezvous mission is the location of the rendezvous point. In our work this choice is based on existing results from [17, 31]. In [31], two-dimensional transfers using the restricted three-body model are completed to the Earth-Moon Lagrangian point $L1$. The paper also suggests that $L1$ serves as a natural gateway to other transfer destinations, such as a parking orbit around the Moon. Moreover, this approach was implemented in [17] and proved successful for generating rendezvous with TCO. For these reasons, we choose to continue to focus on rendezvous near the $L_1$ point, as we did in [17]. An obvious extension for future work would be to select rendezvous points elsewhere on the TCO orbits. We define by $q_{rend}$ the desired rendezvous point on the TCO orbit, which, in this paper, is the point on the TCO orbit that minimizes the Euclidean distance to the $L1$ point. Figure 2 displays the distribution of distances from the rendezvous points of every TCO to the Earth. Notice that the $L1$ point is at a distance of 0.85 LD.

Analysis of the TCO data provides more understanding of how the TCO and $L1$ are related. We see that 12,561 TCO come within 1 Lunar Distance (LD) of the $L1$ point, and that 386 come within 0.1 LD of the $L1$ point, (note, one Lunar Distance (LD) is defined as 384,400 km, an approximate average distance between the Earth and the Moon). In [17], transfers were attempted to a sample of 100 TCO chosen from those 386 TCO.

| TCO # | $d_{L1}$ (LD) | $d_{Earth}$ (LD) | $\lvert v_{rend}\rvert$ (LD/d) | $t_{rend}$ (d) | $T_{capt}$ (d) | $n_{orbits}$ |
|---|---|---|---|---|---|---|
| 1 | 1.46 | 2.30 | 0.17 | 180.53 | 452.16 | -2.88 |
| 2 | 1.97 | 2.63 | 0.17 | 239.20 | 285.65 | -1.84 |
| 3 | 0.85 | 0.25 | 0.72 | 59.51 | 139.96 | -1.45 |
| 4 | 0.60 | 0.25 | 0.59 | 33.80 | 70.06 | -1.11 |
| 5 | 0.37 | 0.72 | 0.36 | 21.26 | 85.94 | -1.17 |
| 6 | 0.60 | 1.40 | 0.27 | 97.03 | 197.79 | -1.41 |
| 7 | 1.06 | 1.18 | 0.30 | 28.22 | 168.07 | -1.25 |
| 8 | 1.31 | 1.93 | 0.23 | 109.44 | 513.73 | -2.74 |
| 9 | 0.36 | 0.88 | 0.32 | 151.98 | 182.29 | 1.31 |
| 10 | 1.15 | 1.81 | 0.21 | 261.97 | 359.72 | -2.81 |
| 11 | 2.61 | 3.42 | 0.17 | 81.18 | 303.15 | -1.93 |
| 12 | 0.90 | 1.23 | 0.26 | 78.78 | 206.05 | -1.32 |
| 13 | 0.50 | 0.57 | 0.38 | 342.51 | 508.83 | -1.12 |
| 14 | 0.45 | 0.52 | 0.44 | 82.00 | 153.16 | -1.31 |
| 15 | 0.63 | 0.23 | 0.64 | 114.89 | 136.53 | -1.33 |
| 16 | 0.16 | 0.80 | 0.29 | 308.46 | 1,506.92 | 16.82 |
| 17 | 0.42 | 1.06 | 0.30 | 173.23 | 448.26 | -1.46 |
| 18 | 0.73 | 1.57 | 0.23 | 109.94 | 217.82 | -1.32 |
| 19 | 0.23 | 0.75 | 0.33 | 421.80 | 517.89 | -4.76 |
| 20 | 0.25 | 0.76 | 0.35 | 81.19 | 125.49 | -1.32 |

TABLE 1. Capture statistics for a sample of 20 TCO from the database [23]. Column 3 gives the Euclidean distance $d_{L1}$ in LD between the TCO rendezvous point $q_{rend}$ and $L1$, and similarly, column 4 gives the Euclidean distance $d_{Earth}$ in LD between the TCO rendezvous point $q_{rend}$ and Earth. Column 5 gives the time $t_{rend}$ in days after initial capture that $q_{rend}$ occurs. Column 6 displays the total amount of time $T_{capt}$ in days that the TCO is captured, and column 7 gives the number of orbits $n_{orbits}$ the TCO makes around the Earth while captured.

On Table 1, we provide data for a sample of 20 TCOs that present very different features as it can be observed from the table. For all but one of the TCO in the table, successful transfers are found using the methodology described in this paper. The corresponding thrust and more information about these transfers can be found in Table 2. Notice that no transfer to $q_{rend}$ has been found within the thrust constraint of our spacecraft to TCO #3. This seems to be due to the high velocity of the TCO at this location, being unable to be matched by the spacecraft. This suggests further study to refine the choice of $q_{rend}$ to take into account the velocity as well.

## 3. **Orbital Transfers.**

3.1. **Background.** Mathematical modeling of orbital transfers is a major aspect of designing and executing space missions. The understanding of the mathematical properties of the celestial systems and of the possible space trajectories to be used by a spacecraft enables the completion of missions along with minimizing the use

of correction maneuvers, the transfer time or the propellant cost. Since the start of space exploration in the second half of the twentieth century, tremendous progress has been made in developing mathematical tools for modeling accurate, feasible and efficient orbital transfers. The theoretical study of Newton's laws of universal gravitation [30], on which classical mechanics is based, permits the generation of the well-known Hohmann and bi-elliptic transfers [38], notably used during the Apollo program to bring a spacecraft from a low-Earth circular orbit to a higher one by minimizing the so-called change of velocity $\Delta v$. Over the last two decades, the application of theory of dynamical systems to astrodynamics has enabled the construction of new types of low-energy transfers. This includes, in particular, brilliant methods based on chaotic motion in celestial mechanics, presented in details in [6] and successfully put into practice to rescue the Japanese spacecraft Hiten [7]. Other techniques take advantage of the structure of invariant manifolds of the collinear equilibrium points for the restricted three-body problem [37] to construct, *inter alia*, low-energy transfers following a prescribed itinerary between a planet and its moons [21]. The design of the Genesis discovery mission [22] relies, for instance, on this idea.

Optimal control theory also provides powerful results to classify and study the geometric characteristics, and to compute time-minimizing or energy-minimizing transfers. This is this approach that we adopt in this paper. Numerous and various kinds of optimal transfers have been simulated in the last fifteen years, by means of both direct and indirect methods in optimal control, in the two, three or four-body problems [5, 8, 16, 20, 29, 31]. In particular, optimal transfer strategies for the Smart-1 mission from the European Space Agency [33, 34] are proposed in [19]. In this article, we present a principle of using indirect numerical methods to compute an exhaustive collection of time-minimal transfers from the geostationary orbit to TCO.

3.2. **Geometric Optimal Control.** The numerical methods developed in this article for computing time-minimal transfers from the geostationary orbit to TCO are based on theoretical results from optimal control theory [2, 11, 24, 27], the central one being the *Pontryagin Maximum Principle* [32]. This fundamental theorem provides necessary conditions for a solution of a control system to be optimal, with respect to a given integral cost, and can be stated as follows. Let $V$ be an open subset of $\mathbb{R}^n$, $U$ an open subset of $\mathbb{R}^m$ and let us consider a general control system

$$\left\{ \begin{array}{c} \dot{q}(t) = f(q(t), u(t)) \\ \min_{u(.)} \int_0^{t_f} f^0(q(t), u(t))dt \\ q(0) = q_0 \in M_0,\ q(t_f) \in M_1 \end{array} \right. \tag{1}$$

where $f : V \times U \longrightarrow$ and $f^0 : V \times U \longrightarrow \mathbb{R}$ are smooth, $u(.)$ is a bounded measurable function defined on $[0, t(u)] \subset \mathbb{R}^+$ valued in $U$, $t_f < t(u)$ and $M_0$ and $M_1$ are two subsets of $\mathbb{R}^n$. We call an *admissible control on* $[0, t_f]$ a control $u(.)$ whose corresponding trajectory $q(.)$ satisfies $q_0 \in M_0$ and $q(t_f) \in M_1$. Then, for an admissible control $u(.)$ to be optimal, there necessarily exists a non-positive real $p^0$ and an absolutely continuous map $p(.)$ on $[0, t_f]$, called the *adjoint vector*, such that $p(t) \in \mathbb{R}^n$, $(p^0, p) \neq (0, 0)$ and, almost everywhere on $[0, t_f]$, there holds

$$\dot{q}(t) = \frac{\partial H}{\partial p}(q(t), p(t), p^0, u(t)),\ \dot{p}(t) = -\frac{\partial H}{\partial q}(q(t), p(t), p^0, u(t)), \tag{2}$$

where $H$ is the so-called *pseudo-Hamiltonian* function defined by

$$\begin{aligned} H : V \times \mathbb{R}^n \times \mathbb{R}^*_- \times U &\longrightarrow \mathbb{R} \\ (q, p, p^0, u) &\longrightarrow p^0 f^0(q, u) + < p, f(q, u) > . \end{aligned}$$

Moreover, the maximization condition

$$H(q(t), p(t), p^0, u(t)) = \max_{v \in U} H(q(t), p(t), p^0, v) \tag{3}$$

is satisfied almost everywhere on $[0, t_f]$. Lastly, the transversality conditions implies that if $M_0$ (resp. $M_1$) is a regular submanifold of $\mathbb{R}^n$, then

$$p(0) \perp T_{q(0)} M_0 \quad (\text{resp.} \quad p(t_f) \perp T_{q(t_f)} M_1). \tag{4}$$

where $T_{q(0)} M_0$ (resp. $T_{q(t_f)} M_1$) is the tangent plan of $M_0$ (resp. $M_1$) at $q(0)$ (resp. $q(t_f)$). We call an *extremal curve* a solution $(q, p, p^0, u)$ of equations (2) and (3). Notice that since $U$ is an open set of $\mathbb{R}^m$, the maximization condition 3 can be written $\frac{\partial H}{\partial u} = 0$. Let's assume that this expression of the maximization condition implies that any extremal control in a neighborhood of $u(.)$ is a smooth feedback function of the form $u_r(t) = u_r(q(t), p(t))$. The pseudo-Hamiltonian $H$ can thus be written as a real Hamiltonian function $H_r(q, p) = H(q, p, p^0, u_r(q, p))$ and any extremal trajectory can be expressed as a solution $z = (q, p)$ of the Hamiltonian system

$$\begin{cases} \dot{q}(t) = \dfrac{\partial H_r}{\partial p}(q(t), p(t)), \ \dot{p}(t) = -\dfrac{\partial H_r}{\partial q}(q(t), p(t)) \\ (q(0), p(0)) = (q_0, p_0). \end{cases} \tag{5}$$

In this context, any solution of the optimal control problem (1) is, consequently, necessarily the projection of an extremal curve solution of the Hamiltonian system (5). Thus, extremal curves provide candidate trajectories for being optimal solutions of (1).

*Second order optimality condition* have been derived for constrained control and state, see [15, 28, 39] for instance. In our work, we consider the unconstrained situation when computing the second order optimality condition. The condition therefore reduces to the analysis of conjugate points as described in [1, 10, 13, 36]. To the Hamiltonian system (5), let us associate the *Jacobi equation* equation on $\mathbb{R}^n$

$$\delta\dot{q}(t) = d\frac{\partial H_r}{\partial p}(q(t), p(t)).\delta q(t), \ \delta\dot{p}(t) = -d\frac{\partial H_r}{\partial q}(q(t), p(t)).\delta p(t) \tag{6}$$

along an extremal $z(.) = (q(.), p(.))$. A *Jacobi field* is a nontrivial solution $J(t) = (\delta q(t), \delta p(t))$ of (6) along $z(.)$. A Jacobi field is said to be *vertical* at time $t$ if $\delta q(t) = 0$. A time $t_c$ is said to be a *geometrically conjugate time* if there exists a Jacobi field which is vertical at 0 and at $t_c$. Then, $q(t_c)$ is said to be *conjugate* to $q(0)$. Conjugate times can be geometrically characterized by considering the *exponential mapping* which is defined, when the final time is free (such as in the time minimization problem) by

$$\exp_{q_0, t} : p_0 \longrightarrow q(t, q_0, p_0) \tag{7}$$

where $q(t, q_0, p_0)$ is the projection on the phase space of the solution of (5) evaluated at the time $t$. We denote $\exp_t(\frac{\partial H_r}{\partial p}, -\frac{\partial H_r}{\partial q})$ the flow of the vector field $(\frac{\partial H_r}{\partial p}, -\frac{\partial H_r}{\partial q})$. The following proposition results from a geometrical interpretation of the Jacobi equation, see [10] for a detailed proof. In our case the manifold $M$ is identified to $\mathbb{R}^n$ and $T^*_{q_0} M$ denotes the cotangent space at $q_0$.

**Theorem 3.1.** *Let $q_0 \in M$, $L_0 = T^*_{q_0}M$ and $L_t = \exp_t(\frac{\partial H_r}{\partial p}, -\frac{\partial H_r}{\partial q}))(L_0)$. Then $L_t$ is a Lagrangian submanifold of $T^*M$ whose tangent space is spanned by Jacobi fields starting from $L_0$. Moreover $q(t_c)$ is geometrically conjugate to $q_0$ if and only if $\exp_{q_0,t_c}$ is not an immersion at $p_0$.*

Under generic assumptions, the following theorem connects the notion of conjugate time and the local optimality of extremals, see for instance [1, 10, 13] for greater details.

**Theorem 3.2.** *Let $t_c^1$ be the first conjugate time along $z(.)$. The trajectory $q(.)$ is locally optimal on $[0, t_c^1)$ in $L^\infty$ topology. If $t > t_c^1$ then $q(.)$ is not locally optimal on $[0, t]$.*

3.3. **Indirect Methods.** As stated in the section 3.2, extremal curves are solutions of a true Hamiltonian system, satisfying given boundary conditions and derived from the application of the Pontryagin Maximum Principle. They can be numerically computed by means of the so-called *indirect methods*. The main difficulty to overcome consists of determining the initial value of the adjoint vector $p_0$ such that the boundary conditions are satisfied. Rewriting the boundary and transversality conditions under the form $R(q(0), p(0), q(t_f), p(t_f)) = \vec{0}$, admissible extremals can be expressed as solutions of

$$\begin{cases} \dot{q}(t) = \frac{\partial H_r}{\partial p}(q(t), p(t)),\ \dot{p}(t) = -\frac{\partial H_r}{\partial q}(q(t), p(t)) \\ R(q(0), p(0), q(t_f), p(t_f) = \vec{0}. \end{cases} \tag{8}$$

When the transfer time $t_f$ is free, solving the boundary value problem is then equivalent to finding a zero of the so-called *shooting function* [12] $S$ defined by

$$S : (p_0, t_f) \longrightarrow R(z_0, z_{t_f}). \tag{9}$$

In the free final time situation, the condition $H_r = 0$, deduced from the application of the Pontryagin Maximum principle [32], is added to the function $R$. By construction $S$ is a smooth function, and a Newton type algorithm can be used to determine its zeroes.
Newtonian methods, however, are very sensitive to the initial guess, which must be chosen accurately. To do so, we use a *smooth continuation method* [3]. This technique is based on connecting the Hamiltonian $H_r$ to an Hamiltonian $H_0$, whose corresponding shooting equation is easy to solve, via a parametrized family $(H_\lambda)_{\lambda\in[0,1]}$ of smooth Hamiltonians. The algorithm then is divided into the following steps:

1. Firstly, we solve the shooting equation associated with $H_0$;
2. We then set up a discretization $0{=}\lambda_0, \lambda_1, \ldots, \lambda_N{=}1$ and solve iteratively the shooting equation associated with $H_{\lambda_{i+1}}$ by using as initial guess the solution of the shooting equation corresponding to $H_{\lambda_i}$.
3. The solution of the last shooting equation associated with $H_{\lambda_N}$ is consequently a zero of the shooting function $S$.

Let us mention that for the smooth continuation method to converge, we must verify at every step of the algorithm that the first conjugate point $t_c$ along the generated extremal curve is greater than the final time $t_f$, see [14].
The software Hampath, see [18], is designed along the method described above and allows one to check the second order optimality condition when smooth optimal control problems are considered.

4. **Rendezvous Missions to Temporarily-Captured Natural Earth Satellites.** In this section we apply the method described in section 3 to design rendezvous mission to TCOs. A small sample of such missions has been calculated successfully in [17]. The main goal of this paper is to determine the percentage of TCOs, from the catalogue of over sixteen-thousand TCOs computed in [23], to which we can design a rendezvous mission and to determine the lowest possible thrust within our constraints using a continuation method.

4.1. **Mathematical Model.** As a first approach, we consider time-minimal transfers from the geostationary orbit to TCO as space trajectories within the Earth-Moon system. Due to the small eccentricity of the orbit of the Moon around the Earth, we choose to model the motion of the spacecraft in the Earth-Moon system using the equations of the restricted three-body problem. Neglecting the influence of the other planets is justified by the fact that during the transfer, the natural satellite to reach is temporarily captured by the Earth. On Figure 3 we represent the distance between the orbits of the TCOs obtained using our model when initialized from the rendezvous point and the ones computed in [23] to determine the accuracy of our approximation. While it can be observed on specific TCOs that the model presents some significant discrepancies with the initial orbits, for a large percentage of the TCOs the restricted three-body model provides a satisfactory approximation which therefore motivates this first study.

This classical model is derived from the Newton's law of universal gravitation, [30]. It describes the three-dimensional motion of a celestial object with negligeable mass (the spacecraft), subjected to the gravitational fields of two main bodies called *primaries* (the Earth and the Moon), revolving in circular orbits at constant angular velocity 1 around their center of mass $G$ under the influence of their mutual gravitational attraction. We normalize the respective mass $M_1$ and $M_2$ of the Earth and the Moon so that $M_1 + M_2 = 1$ and denote $\mu = \frac{M_2}{M_1+M_2} \in [0, \frac{1}{2}]$ the reduced mass of the problem. For the Earth and Moon, $\mu = 0.01215361914$. Using a rotating coordinates system centered at $G$ with an angular velocity 1, the Earth and the Moon are respectively located at the fixed locations $(-\mu, 0, 0)$ and $(1-\mu, 0, 0)$. Let us denote $(x(t), y(t), z(t))$ the spatial position of the spacecraft at time $t$. In the rotating coordinates system, the equations of the free motion of the spacecraft are written [37]

$$\ddot{x} - 2\dot{y} = \frac{\partial V}{\partial x}, \ \ddot{y} + 2\dot{x} = \frac{\partial V}{\partial y}, \ \ddot{z} = \frac{\partial V}{\partial z}, \tag{10}$$

where $-V$ is the mechanical potential given by

$$V = \frac{x^2 + y^2}{2} + \frac{1-\mu}{\varrho_1} + \frac{\mu}{\varrho_2} + \frac{\mu(1-\mu)}{2}, \tag{11}$$

with $\varrho_1 = \sqrt{\left((x+\mu)^2 + y^2 + z^2\right)}$, $\varrho_2 = \sqrt{\left((x-1+\mu)^2 + y^2 + z^2\right)}$ representing the distances from the spacecraft to the primaries. This dynamical system has five equilibrium points defined as the critical points of the potential $V$. They are all located in the $(x, y)$ plane and divided in two different types. The *Euler points*, denoted $L_1$, $L_2$ and $L_3$, located on the line $y = 0$ defined by the primaries, are non-stable, according to the Arnold's stability theorem [4]. The *Lagrange points* $L_4$ and $L_5$ each form an equilateral triangle with the two primaries. They are stable when $\mu$ satisfies the inequality $\mu < \mu_1 = \frac{1}{2}(1 - \frac{\sqrt{69}}{9})$ which is the case for the Earth-Moon system. The influence of the propulsion provided by the thrusters on the motion

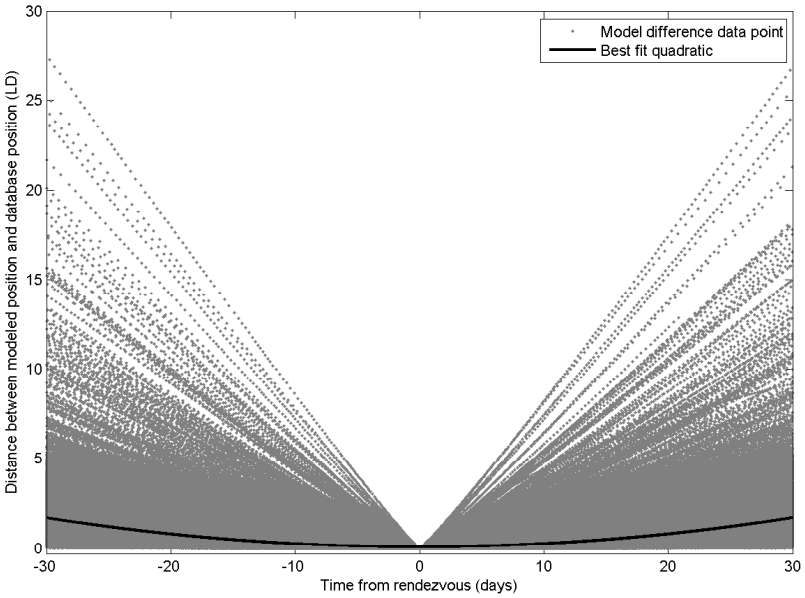


FIGURE 3. A representation of the accuracy of the model. The trajectory of each TCO in the database is integrated, for 30 days before and after its rendezvous point, using the restricted three-body model. The results are then compared to the original data from the database [23], which was obtained using a more sophisticated model. The quadratic of best fit (in a least squares sense) is plotted to represent the relationship between the model we used and the supplied data.

of the spacecraft is modelled by adding control terms in the equation (10). The motion of the spacecraft is therefore completely described by the control system

$$\ddot{x} - 2\dot{y} = \frac{\partial V}{\partial x} + u_1,\ \ddot{y} + 2\dot{x} = \frac{\partial V}{\partial y} + u_2,\ \ddot{z} = \frac{\partial V}{\partial z} + u_3. \tag{12}$$

where $u(.) = (u_1(.), u_2(.), u_3(.))$ is the control. The constraint on the thrust translates into the domain of control as $U = B_{\mathbb{R}^3}(0, \epsilon)$ where $\epsilon$ is the maximum thrust. Using the phase space variable $q = (x, y, z, \dot{x}, \dot{y}, \dot{z})$, the system (12) can be rewritten

$$\dot{q} = F_0(q) + F_1(q)u_1 + F_2(q)u_2 + F_3(q)u_3 \tag{13}$$

where

$$F_0(q) = \begin{pmatrix} q_4 \\ q_5 \\ q_6 \\ 2q_5 + q_1 - (1-\mu)\frac{q_1+\mu}{((q_1+\mu)^2+q_2^2+q_3^2)^{\frac{3}{2}}} - \mu\frac{q_1-1+\mu}{((q_1-1+\mu)^2+q_2^2+q_3^2)^{\frac{3}{2}}} \\ -2q_4 + q_2 - (1-\mu)\frac{q_2}{((q_1+\mu)^2+q_2^2+q_3^2)^{\frac{3}{2}}} - \mu\frac{q_2}{((q_1-1+\mu)^2+q_2^2+q_3^2)^{\frac{3}{2}}} \\ -(1-\mu)\frac{q_3}{((q_1+\mu)^2+q_2^2+q_3^2)^{\frac{3}{2}}} - \mu\frac{q_3}{((q_1-1+\mu)^2+q_2^2+q_3^2)^{\frac{3}{2}}} \end{pmatrix}$$

$$F_1(q) = \begin{pmatrix} 0 \\ 0 \\ 0 \\ 1 \\ 0 \\ 0 \end{pmatrix}, \; F_2(q) = \begin{pmatrix} 0 \\ 0 \\ 0 \\ 0 \\ 1 \\ 0 \end{pmatrix}, \; F_3(q) = \begin{pmatrix} 0 \\ 0 \\ 0 \\ 0 \\ 0 \\ 1 \end{pmatrix}.$$

Computing time-minimal transfer from the geostationary orbit to a given TCO is then equivalent to solving the optimal control problem

$$\begin{cases} \dot{q} = F_0(q) + F_1(q)u_1 + F_2(q)u_2 + F_3(q)u_3 \\ \min_{u(\cdot)\in B_{\mathbb{R}^3}(0,\epsilon)} \int_{t_0}^{t_f} dt \\ q(0) \in \mathcal{O}_g, \; q(t_f) = q_{rend} \end{cases}. \tag{14}$$

where $\mathcal{O}_g$ is the geostationary orbit described as a 1-sphere embedded in $\mathbb{R}^3$, $q_{rend}$ is the imposed final condition representing the position and velocity at which we want the spacecraft to rendezvous with the TCO and $\epsilon$ is the control bound corresponding to the maximal thrust allowed by the spacecraft engines.

4.2. **Methodology.** Applying the Pontryagin Maximum Principle, we find that, in the so-called *normal case* $p_0 \neq 0$, every solution $q(.)$ of (14) is the projection of an extremal curve $z(.) = (q(.), p(.))$ solution of the Hamiltonian system

$$\dot{q}(t) = \frac{\partial H}{\partial p}, \; \dot{p}(t) = -\frac{\partial H}{\partial q} \tag{15}$$

where

$$H(q,p,u) = -1 + H_0(q,p) + \epsilon((u_1 H_1(q,p) + u_2 H_2(q,p) + u_3 H_3(q,p))$$

with $H_i(q,p) = \langle p, F_i(q)\rangle$, $i = 1,2,3$. From the maximization condition, we find that, if $(H_1, H_2, H_3) \neq (0,0,0)$, then the control $u(.)$ satisfies

$$u_i(q,p) = \frac{H_i(q,p)}{\sqrt{H_1^2(q,p) + H_2^2(q,p) + H_3^2(q,p)}}, \quad i = 1,2,3. \tag{16}$$

Plugging into $H$ gives the expression of the real Hamiltonian

$$H_r(q,p) = -1 + H_0(q,p) + \epsilon((H_1^2(q,p) + H_2^2(q,p) + H_3^2(q,p))^{\frac{1}{2}})$$

whose the corresponding extremals, solutions of the system

$$\dot{q}(t) = \frac{\partial H_r}{\partial p}, \; \dot{p}(t) = -\frac{\partial H_r}{\partial q} \tag{17}$$

are called *order zero extremals*. The final time being free, $H_r$ is identically zero on $[0, t_f]$, see [32], and the computation of time-minimal order 0 extremal transfers can therefore be carried out by solving the shooting equation associated with the function

$$\begin{aligned} S : \mathbb{R}^7 &\longrightarrow \mathbb{R}^7 \\ (p_0, t_f) &\longrightarrow \begin{pmatrix} q(t_f) - q_{rend} \\ H_r(q(t_f), p(t_f)) \end{pmatrix}. \end{aligned}$$

Let us mention however that this method may provide higher order extremal transfers along which appear singularities. Indeed, it can be proved, see [9], that such singularities are isolated and only occur a finite number of times. The variable stepsize algorithm, provided by the software Hampath, may or may not handle such singularities while computing of extremal transfers. The initial position and

velocity on the geostationary orbit are set as $q_0 = (0.0947, 0, 0,\ 0, 2.8792, 0)$, the mass of the spacecraft being assumed constant to 350 kg. Our computations follow the hereafter principle. First, we compute a collection of three-dimensional 1N-thrust time-optimal transfers to the 100 TCO coming within 0.1 Lunar units of the point $L_1$ with the smallest absolute vertical coordinate $z$, choosing as the rendezvous location the point they are nearest to $L_1$. Indeed, as explained in details in [17], those three-dimensional time-optimal extremal curves can be computed by using the two-dimensional time-optimal extremal curves from the geostationary orbit to the projection of the selected TCO on the plane of motion of the Moon around the Earth as an initial guess for the shooting method to converge. Let us mention that these two-dimensional extremal curves have been previously computed by initializing a shooting method with a reference time-optimal transfer to the point $L_1$ provided in [31]. The first conjugate time along every three-dimensional generated extremal is computed to ensure, according to the second order condition, that it is locally time-optimal (see Theorem (3.2)).
This collection of one hundred 1N-thrust time-optimal transfers is then used to set up a database of initial guesses to compute 1N-thrust time-minimal transfers to the remaining TCOs. For a given TCO denoted $\mathcal{TCO}_1$, we define as the rendezvous location the point $q_{1,rend}$ at which $\mathcal{TCO}_1$ is nearest the point $L_1$. We then search among the database of initial guesses for the time-minimal transfer which realizes a rendezvous with a TCO denoted $\mathcal{TCO}_2$ at the location denoted $q_{2,rend}$ such that the Euclidean norm $\|q_{1,rend} - q_{2,rend}\|_2$ is minimized. This transfer is used as the initial guess for the shooting equation to compute a time-minimal extremal curve to rendezvous with $\mathcal{TCO}_1$, and the first conjugate point along this extremal is computed to guarantee its local time-optimality. The database of initial guesses is afterwards updated with this new time-minimal transfer. If either the shooting method or the second order condition fails, $\mathcal{TCO}_1$ is placed back in the set of TCO for which no transfer has been calculated and the algorithm will retry to compute a time-minimal transfer to $\mathcal{TCO}_1$ after having attempted computing time-minimal transfers to the other TCO and expanded the database of initial guesses. This method allows us to successfully realize rendezvous missions for more than 96% of the TCOs with a maximal thrust of 1N. See section 5 below for more results.
Once a 1N-thrust time-minimal transfer has been computed to a given TCO, a discrete homotopic method on the parameter $\epsilon$, can then be used to determine solutions of the shooting function for smaller control bounds, and thus, lower thrust extremal curves from the geostationary orbit to $q_{rend}$. Indeed, the higher the maximum control bound, the shorter the corresponding transfer time and the more easily the Newton algorithm converges to a solution of the shooting method, which makes this problem well suited for a continuation method. At each step of the continuation algorithm, the first conjugate time along every generated extremal is computed to ensure both the convergence of the smooth continuation method and the local time-optimality of the extremal curve.
Most of the numerical methods described in this section have been performed using the software *HAMPATH : on solving optimal control problems by indirect and path following methods*, http://apo.enseeiht.fr/hampath/ .

5. **Results.** Using the methodology described above, 1N transfers were found to 16,352 of the 16,923 TCOs. The successful 1N transfers were used as starting points to find 250 transfers with lower maximum thrust bounds (between 0.1N and 1N).

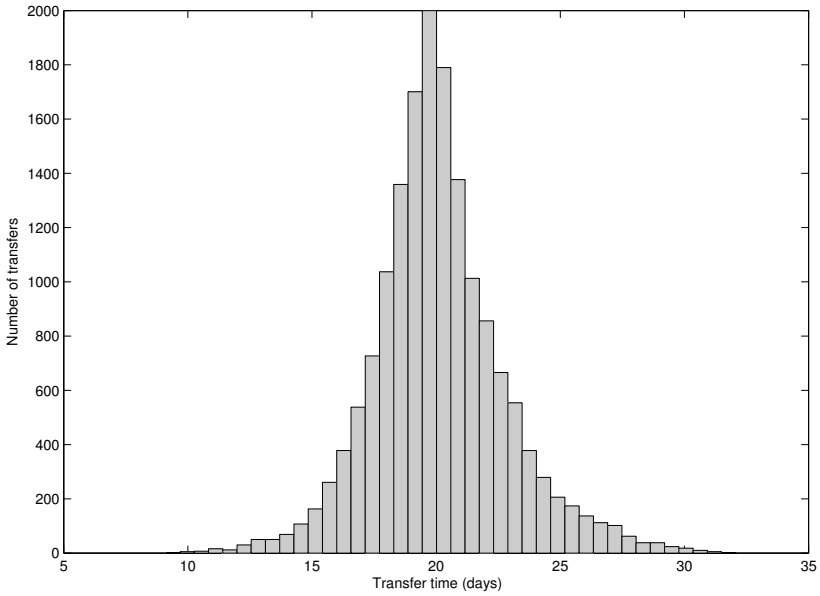


FIGURE 4. A histogram representing the distribution of 1N transfer times in days.

The computations for the 1N transfers took nine days to run on a single laptop. The continuation computations took much longer, at about approximately 30-45 minutes per TCO, again running on a single laptop.

5.1. **1N transfers.** Our methodology successfully determined transfers to 96.6% of the rendezvous points we attempted to transfer to. The shortest identified transfer time was 9.11 days, and the longest was 32.10 days. The mean transfer time was found as 20.12 days, and the median transfer time was 19.92 days. Figure 4 displays the distribution of 1N transfer times.

Illustrations of transfers are shown in the next section, in Figures 7-11, plot (b), for five distinct TCO. To represent our results we use a three-dimensional view as well as two-dimensional projection. The five distinct 1N-transfers illustrate the variation in the TCO's orbits. It can be observed, for instance, that the shortest time transfer of the five displayed is obtained for TCO #16 which revolves around the Earth a greater number of times. The reader should keep in mind that the velocity of the TCO at $q_{rend}$ plays an important role in the transfer. We plan on conducting a more detailed analysis in future work.

We provide a brief preliminary analysis of the TCO for which we did not identify a transfer. Figure 5 demonstrates that the rendezvous points for which we did not obtain transfers to were typically close to Earth, with relatively high velocities. Figure 6 gives a histogram of the number of rendezvous points with respect to their distance from Earth, sorted by rendezvous points we did and did not find transfers for. It is clear from the figures that most of the rendezvous points that we did not find transfers to are within 0.2LD of Earth, with velocities upwards of 0.6LD/d. The

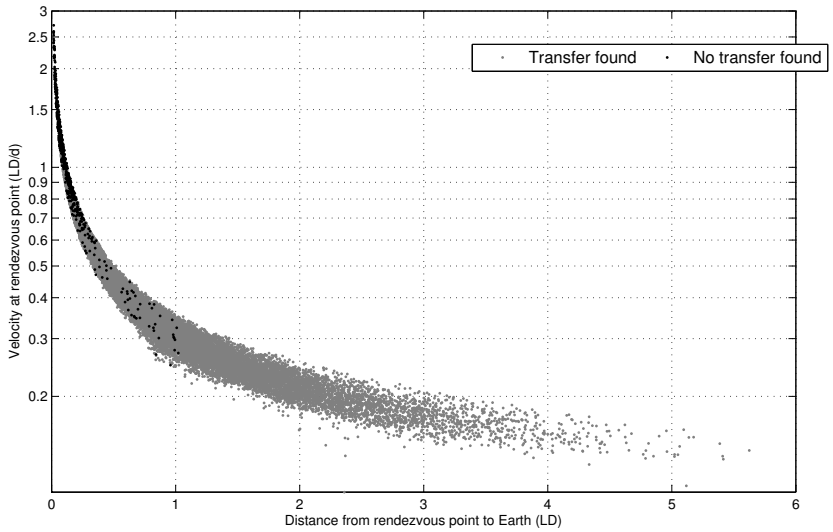


FIGURE 5. A scatterplot representing the rendezvous points which we did (gray) and did not (black) obtain transfers to.

high velocities of the rendezvous points which were unreachable with our method seem to be unreachable because of the spacecraft's thrust constraint. We expect that with a higher admissible thrust we could reach 100% of the TCO using our methodology.

5.2. **Continuations to lower thrusts.** For a random selection of the 250 successful 1N transfers, we used a discrete continuation method to search for transfers with a maximum thrust of less than 1N. For each TCO from this random selection, we recorded the lowest maximum thrust bound $\epsilon_{min}$ for which a successful transfer was found. We stress that this was a first approach to lowering the maximum thrust bound, and that these results should be viewed as a first example of what is possible using a simple discrete continuation method.

The lowest $\epsilon_{min}$ found for any transfer was 0.1316N to TCO # 16 (see Figure 10, c) with a transfer time of 103.3 days. For two of the 250 TCO, $\epsilon_{min} = 1$N, meaning the continuation was unable to lower the maximum thrust bound from 1N. The mean value was $\epsilon_{min} = 0.4441$N, and the median value was $\epsilon_{min} = 0.4101$N. Transfer data for the 1N and $\epsilon_{min}$N transfers for the sample of 20 TCOs introduce in Table 1 are presented in Table 2. Notice that TCO #4 has the second highest velocity at $q_{rend}$ (second to TCO #3, which could not be reached even with a 1N bound), has a significant higher $\epsilon_{min}$ than the other TCOs. It can also clearly be observed that the higher the thrust the shorter the duration of the transfer. For comparison, we present in Figures 7-11 illustrations of five successful 1N transfers, and their corresponding $\epsilon_{min}$N transfers. Each transfer is displayed in a three-dimensional plot, as well as an overhead two-dimensional plot. The corresponding transfer times are listed in the captions.

In case it is of interest to the reader, for TCO #16 we provide some specific details of our numerical results. All values are given in the rotating reference frame,

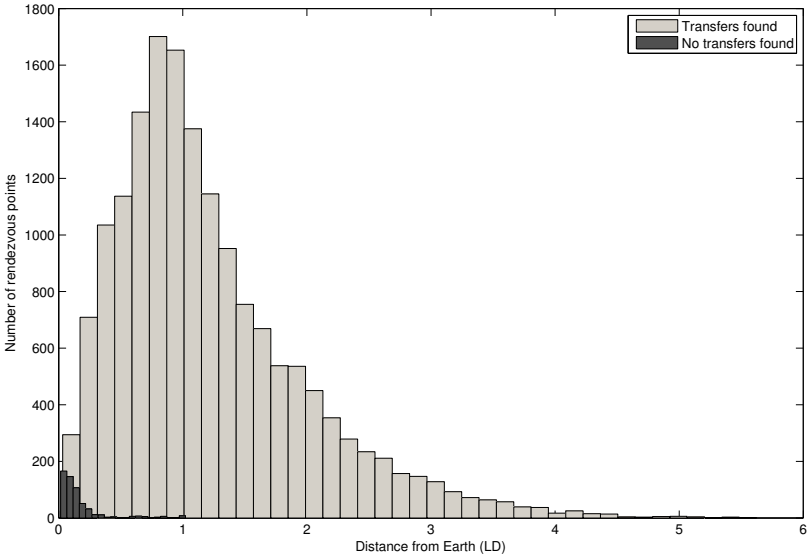


(a) Wide view of histogram

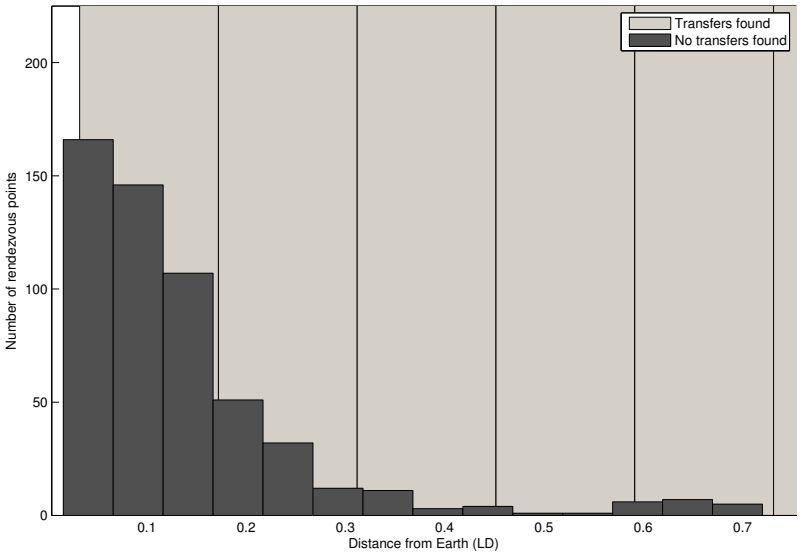


(b) Zoomed view of histogram

FIGURE 6. Histogram showing the distances from rendezvous points to Earth. The data is sorted into two categories: rendezvous points we found transfers to (light gray), and those we did not (dark gray).

| TCO # | $t_f^1$ (d) | $t_c^1$ (d) | $t_{rend} - t_f^1$ (d) | $\epsilon_{min}$ (N) | $t_f^{\epsilon_{min}}$ (d) | $t_c^{\epsilon_{min}}$ (d) | $t_{rend} - t_f^{\epsilon_{min}}$ (d) |
|---|---|---|---|---|---|---|---|
| 1 | 20.88 | $\infty$ | 159.65 | 0.33 | 50.87 | 94.26 | 129.66 |
| 2 | 23.11 | $\infty$ | 216.08 | 0.25 | 76.76 | $\infty$ | 162.44 |
| 3 | - | - | - | - | - | - | - |
| 4 | 17.76 | 21.75 | 16.04 | 0.73 | 25.28 | 23.63 | 8.52 |
| 5 | 18.91 | 28.28 | 2.35 | 0.39 | 43.26 | 54.58 | -22.00 |
| 6 | 20.15 | $\infty$ | 76.87 | 0.46 | 44.76 | 215.87 | 52.27 |
| 7 | 22.59 | 137.14 | 5.63 | 0.36 | 66.68 | 53.74 | -38.46 |
| 8 | 21.27 | $\infty$ | 88.17 | 0.38 | 52.64 | 1,362.74 | 56.80 |
| 9 | 19.21 | 29.37 | 132.77 | 0.29 | 48.96 | 59.87 | 103.01 |
| 10 | 21.78 | $\infty$ | 240.20 | 0.25 | 79.58 | 73.03 | 182.39 |
| 11 | 22.73 | $\infty$ | 58.45 | 0.24 | 74.76 | 96.28 | 6.42 |
| 12 | 18.85 | 27.61 | 59.93 | 0.33 | 60.14 | 73.19 | 18.64 |
| 13 | 19.53 | 25.47 | 322.98 | 0.34 | 56.08 | 66.50 | 286.42 |
| 14 | 18.60 | 22.62 | 63.40 | 0.46 | 37.36 | 43.77 | 44.64 |
| 15 | 17.72 | 29.47 | 97.17 | 0.59 | 26.82 | 42.74 | 88.07 |
| 16 | 13.40 | 20.07 | 295.06 | 0.13 | 103.31 | 121.58 | 205.15 |
| 17 | 20.46 | 24.54 | 152.78 | 0.84 | 28.88 | 29.33 | 144.36 |
| 18 | 19.97 | 152.95 | 89.97 | 0.43 | 46.03 | 70.98 | 63.91 |
| 19 | 20.28 | 29.69 | 401.52 | 0.25 | 75.81 | 77.33 | 345.99 |
| 20 | 17.52 | 1,564.12 | 63.67 | 0.56 | 29.29 | 152.65 | 51.89 |

TABLE 2. Transfer statistics for a sample of 20 TCO from the database [23]. Transfers were found for each of the 20 TCO except TCO #3. For the 19 successful, column 2 gives the 1N transfer times $t_f^1$ in days, and column 3 gives the corresponding conjugate times $t_c^1$ in days. Column 4 gives the difference between the TCO time to rendezvous and the transfer time. Note that a negative value in this column means the transfer would be impractical, since we'd have to start the transfer before the TCO was captured (and therefore, likely before it was detected). A continuation method was used to obtain transfers to the same rendezvous points using lower thrusts. Column 5 represents the lowest thrust bound $\epsilon_{min}$ in newtons for which a transfer was found. Columns 6-8 are analogous to columns 2-4, but for the transfer with maximum thrust $\epsilon_{min}$. Note that a conjugate time marked $\infty$ means that no conjugate times were found within 100 times the transfer time.

including the time units for the final time.

$$q_{rend} = \begin{bmatrix} 0.7692503 \\ -0.05583765 \\ 0.1354263 \\ 1.0486000 \\ -0.2893604 \\ 0.3826522 \end{bmatrix}, \; p_0 = \begin{bmatrix} -52.524900 \\ -12.281740 \\ 21.225210 \\ -0.475141 \\ -2.105559 \\ -0.449771 \end{bmatrix}, \; t_f = 23.75782.$$

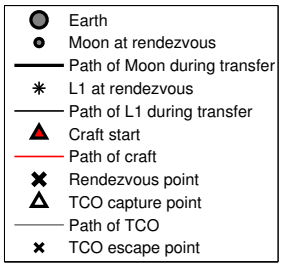


(a) Legend

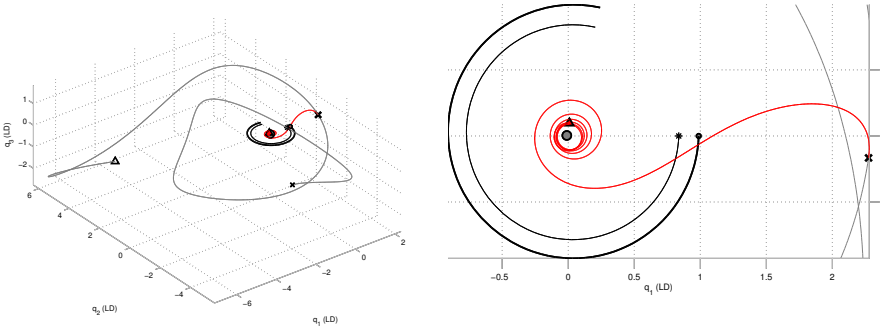

(b) 1N, $t_f$=20.9 days

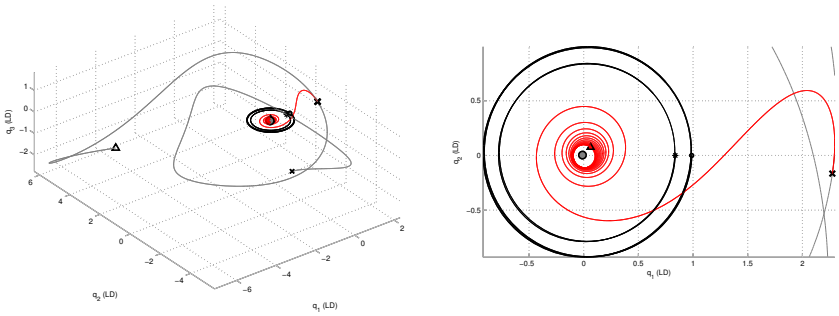

(c) 0.33N, $t_f$=50.9 days

FIGURE 7. (TCO #1) Locally time-minimal transfers associated with two different maximum thrusts – 1N (top) and 0.33N (bottom). Each transfer is displayed with a three dimensional view (left) as well as a overhead two-dimensional view (right). The given legend is applicable to all four plots.

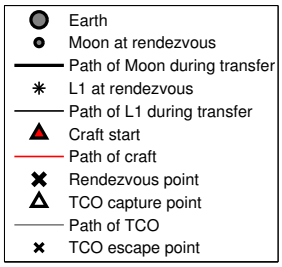


(a) Legend

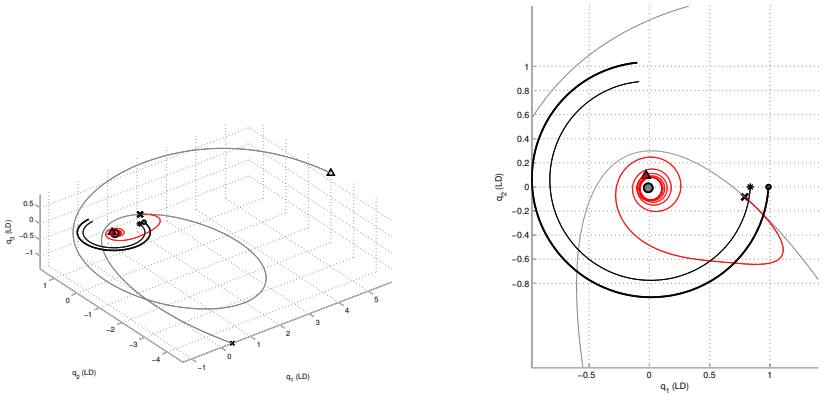

(b) 1N, $t_f$=19.2 days

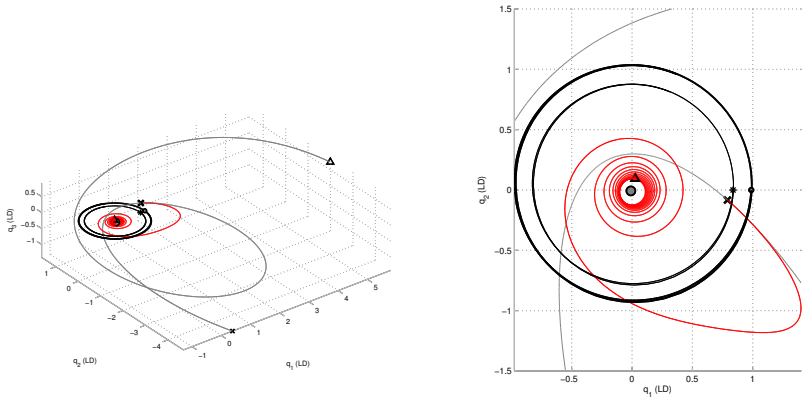

(c) 0.29N, $t_f$=49.0 days

FIGURE 8. (TCO #9) Locally time-minimal transfers associated with two different maximum thrusts – 1N (top) and 0.29N (bottom). Each transfer is displayed with a three dimensional view (left) as well as a overhead two-dimensional view (right). The given legend is applicable to all four plots.

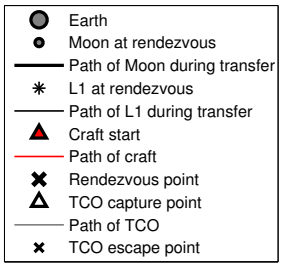


(a) Legend

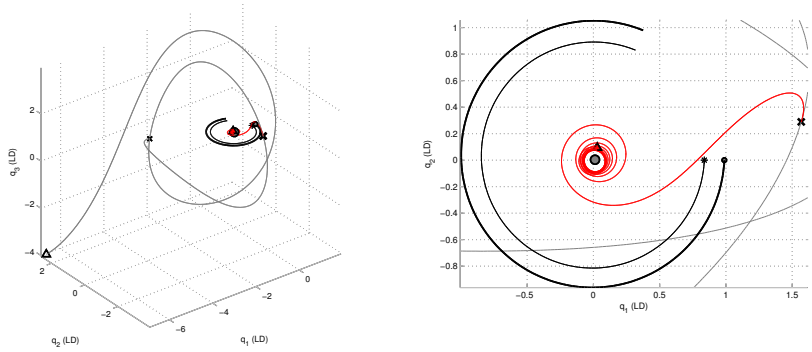

(b) 1N, $t_f$=21.8 days

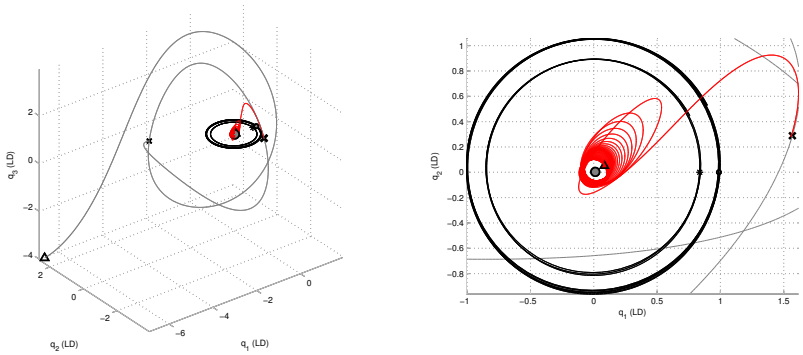

(c) 0.25N, $t_f$=79.6 days

FIGURE 9. (TCO #10) Locally time-minimal transfers associated with two different maximum thrusts – 1N (top) and 0.25N (bottom). Each transfer is displayed with a three dimensional view (left) as well as a overhead two-dimensional view (right). The given legend is applicable to all four plots.

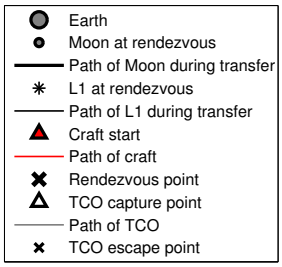


(a) Legend

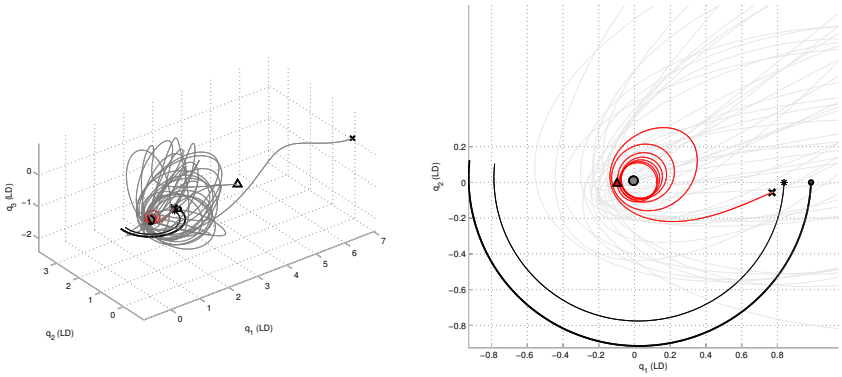


(b) 1N, $t_f$=13.4 days

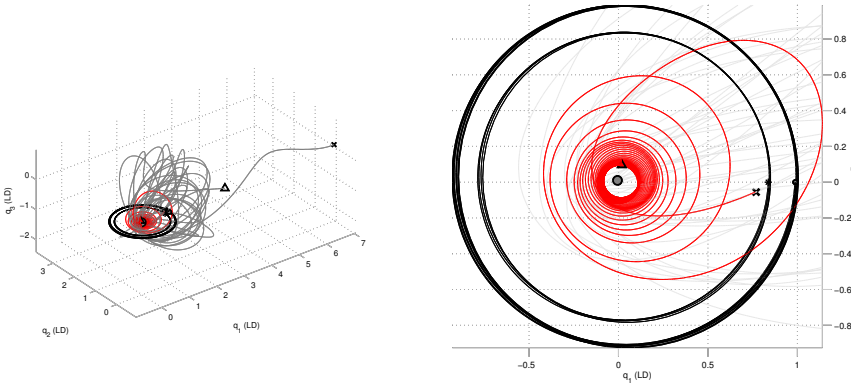


(c) 0.13N, $t_f$=103.3 days

FIGURE 10. (TCO #16) Locally time-minimal transfers associated with two different maximum thrusts – 1N (top) and 0.13N (bottom). Each transfer is displayed with a three dimensional view (left) as well as a overhead two-dimensional view (right). The given legend is applicable to all four plots.

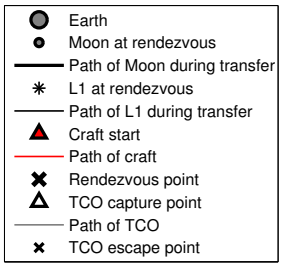


(a) Legend

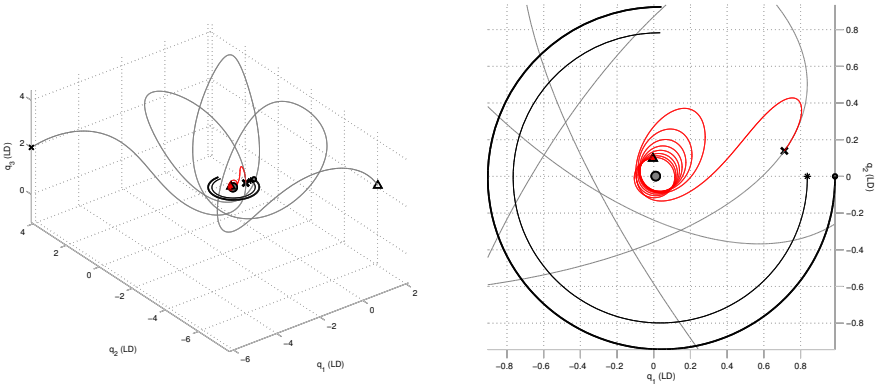

(b) 1N, $t_f$=20.3 days

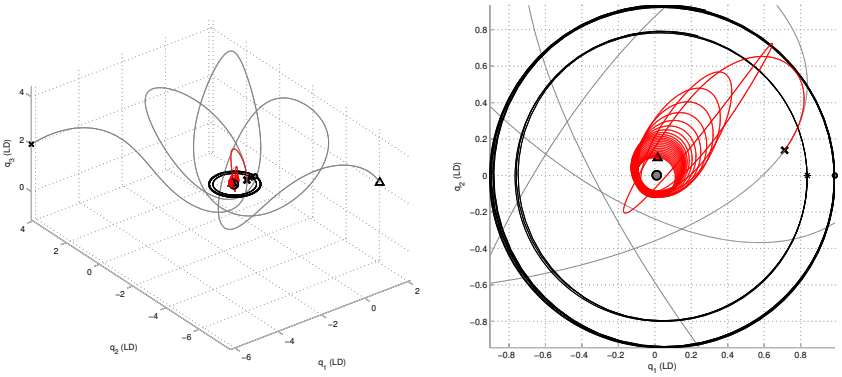

(c) 0.25N, $t_f$=75.8 days

FIGURE 11. (TCO #19) Locally time-minimal transfers associated with two different maximum thrusts – 1N (top) and 0.25N (bottom). Each transfer is displayed with a three dimensional view (left) as well as a overhead two-dimensional view (right). The given legend is applicable to all four plots.

6. **Conclusion and Future Work.** The work presented here is extremely encouraging to pursue further the analysis of rendezvous missions to temporarily-captured natural Earth satellites, or so-called mini-moons. Based on our methodology and techniques from geometric optimal control, we demonstrate the capability to theoretically design low-thrust transfer missions from the geostationary orbit to more than 96% of over sixteen-thousand meteoroids which have theoretically been classified as temporarily captured, in [23]. Refinement of our techniques and model is however necessary for such missions to become a reality. Indeed, first a deeper analysis of the model should be conducted. It has been observed that for some TCOs the approximation with the restricted three-body problem is not satisfactory. It is unknown at this stage what triggers the discrepancy in these cases, and models with an ellipsoidal motion for the Moon or including additional planets will be tested. The location of the rendezvous point of a TCO and the spacecraft is also a major component of our future plan of work. The TCO might actually come closer to the Earth during its capture than it is when closest to the $L1$ point, which therefore suggests that other rendezvous point selection strategies might work better. Additionally as mentioned in this paper, the velocity at the rendezvous point should not be neglected when designing the mission. Finally, the departure point of the spacecraft on the geostationary orbit might as well influence the mission and alternate choices should be studied.

This work opens the door to many interesting and challenging questions, such as catching and grabbing the TCO, followed by a return mission back to Earth.

**Acknowledgments.** This work has been supported by the United States National Science Foundation Division of Graduate Education, award #0841223 and the United States National Science Foundation Division of Mathematical Sciences, award #1109937.

## REFERENCES

[1] A.A. Agrachev and A.V. Sarychev, *On abnormals extremals for Lagrange variational problem*, J. Math. Systems. Estim. Control , **1** (1998), 87–118.
[2] A.A. Agrachev and Y.L. Sachkov, "Control theory from the geometric viewpoint", Springer-Verlag, Berlin, 2004.
[3] E.L. Allgower and K. Georg, "Numerical continuation methods, an introduction", Springer, Berlin, 1990.
[4] V.I. Arnold, "Mathematical methods of classical mechanics", Springer, New-York, 1989.
[5] J.T. Betts and S.O. Erb, *Optimal low thrust trajectories to the Moon*, SIAM J. Appl. Dyn. Syst., **2** (2003), 144–170.
[6] E. Belbruno, "Capture dynamics and chaotic motion in celestial mechanics: with applications to the construction of low energy transfers", Princeton University Press, 2004.
[7] E. Belbruno, "Fly me to the Moon: an insider's guide to the new science of space travel", Princeton University Press, 2007.
[8] B. Bonnard, J.-B. Caillau and G. Picot, *Geometric and Numerical Techniques in Optimal Control of the Two and Three-Body Problems*, Commun. Inf. Syst., **10** (2010), 239–278.
[9] B. Bonnard, J.-B. Caillau and E. Trélat, *Geometric optimal control of elliptic Keplerian orbits*, Discrete Cont. Dyn. Syst. Ser. B, **4** (2005), 929–956.
[10] B. Bonnard, J.-B. Caillau and E. Trélat, *Second order optimality conditions in the smooth case and applications in optimal control*, ESAIM Control Optim. and Calc. Var., **13** (2007), 207–236.
[11] B. Bonnard and M. Chyba, "Singular trajectories and their role in control theory", Springer-Verlag, Berlin, 2003.
[12] B. Bonnard, L. Faubourg and E. Trélat, "Mécanique céleste et contrôle des véhicules spatiaux", Springer-Verlag, Berlin, 2006.

[13] B. Bonnard and I. Kupka, *Théorie des singularités de l'application entrée/sortie et optimalité des trajectoires singulières dans le problème du temps minimal*, (French)[Theory of the singularities of the input/output mapping and optimality of singular trajectories in the minimal-time problem], Forum Math., **2** (1998), 111–159.

[14] B. Bonnard, N. Shcherbakova and D. Sugny, *The smooth continuation method in optimal control with an application to quantum systems*, ESAIM Control Optim. and Calc. Var., **17** (2011), 267–292.

[15] E. Bryson and Y.C. Ho, "Applied optimal control. Optimization, estimation and control. Revised printing.", Hemisphere Publishing Corp. Washington D.C.; Distributed by Halsted Press [John Wiley & Sons] New-York-London-Sydney, 1975.

[16] J.-B. Caillau, "Contribution à l'Etude du Contrôle en Temps Minimal des Transferts Orbitaux", Ph.D thesis, Toulouse University, 2000.

[17] M. Chyba, G. Picot, G. Patterson, R. Jedicke, M. Granvik, J. Vaubaillon "Time-minimal orbital transfers to temporarily-captured natural Earth satellites", OCA5 - Advances in Optimization and Control with Applications Springer Proceedings in Mathematics, To Appear (2013).

[18] J.-B. Caillau, O. Cots and J.Gergaud, *Differential continuation for regular optimal control problems*, Optimization Methods and Software, **27** (2012), no. 2, 177–196.

[19] B. Daoud, "Contribution au Contrôle optimal du problème circulaire restreint des trois corps", Ph.D thesis, Bourgogne University, 2011.

[20] J. Gergaud and T. Haberkorn, *Homotopy method for minimum consumption orbit transfer problem*, ESAIM Control Optim. Calc. Var., **12** (2006), 294–310.

[21] G. Gomez, W.S. Koon, M.W. Lo, J.E. Marsden, J. Masdemont and S.D. Ross, "Invariants manifolds, the spatial three-body problem ans space mission design", Adv. Astronaut. Sci **109** (2001), 3–22.

[22] G. Gomez, W.S. Koon, M.W. Lo, J.E. Marsden, J. Masdemont and S.D. Ross, *Connecting orbits and invariant manifolds in the spatial three-body problem*, Nonlinearity, **17** (2004), 1571–1606.

[23] M. Granvik, J. Vaubaillon, R. Jedicke, *The population of natural Earth satellites*, Icarus, (2012), Vol. 218, 262-277.

[24] V. Jurdjevic, "Geometric control theory", Cambridge University Press, 1997.

[25] J. Kawagachi, A. Fujiwara and T. K. Uesugi, "The ion engine cruise operation and the Earth swingby of Hayabusa (MUSES-C) ", Proceddings of the 55th International Astronotical Congress, Vancouver (2004)

[26] T. Kubota, T. Hashimoto, J. Kawagachi, M. Uo and M. Shirakawa "Guidance and Navigation of Hayabusa spacecraft to asteroid exploration and sample return mission ", Proceddings of SICE-ICASE (2006) 2793–2796

[27] D. Liberzon, "Calculus of variations and optimal control theory. A concise introduction", Princeton University Press, 2012.

[28] H. Maurer, *First and second order sufficient optimality conditions in mathematical programming and optimal control*, Mathematical Programming at Oberwolfach, Math. Programming Stud. **14** (1981), 163–177.

[29] A. Moore, "Discrete mechanics and optimal control for space trajectory design", Ph.D thesis, California Institute of Technology, 2011.

[30] I. Newton, "Principes mathématiques de la philosophie naturelle. Tome I,II (French). Traduction de la marquise du Chastellet, augmentée des commentaires de Clairaut", Librairie scientifique et technique Albert Blanchard, Paris, 1966.

[31] G. Picot, *Shooting and numerical continuation method for computing time-minimal and energy-minimal trajectories in the Earth-Moon system using low-propulsion*, Discrete Cont. Dyn. Syst. Ser. B, **17** (2012), 245–269.

[32] L. S. Pontryagin, V. G. Boltyanskii, R. V. Gamkrelidze and E. F. Mishchenko, "The Mathematical Theory of Optimal Processes", John Wiley & Sons, New York, 1962.

[33] G. Racca, B. H. Foing and M. Coradini, *SMART-1: The first time of Europe to the Moon*, Earth, Moon and planets, **85-86** (2001), 379–390.

[34] G. Racca et al., *SMART-1 mission description and development status*, Planetary and space science, **50** (2002), 1323–1337.

[35] A.G. Santo, S.C Lee and R.E Gold, *NEAR spacecraft and instrumentation*, J. Astronomical Sciences, Vol. 43 **4** (1995), 373–397.

[36] A.V. Sarychev, *Index of second variation of a control system*, Mat. Sb. (N.S), **113** (1980), 464–486.
[37] V. Szebehely, "Theory of Orbits: The Restricted Problem of Three Bodies", Academic Press, 1967.
[38] D.A Vallado, "Fundamentals of astrodynamics and applications", Springer, 2001.
[39] V. Zeidan *First and second order sufficient conditions for optimal control and the calculus of variations*, Appl. Math. and Optim. 11 **3** (1984), 209–226.

Received March 2013; 1st revision May 2013; final revision August 2013.

*E-mail address*: chyba@hawaii.edu
*E-mail address*: gpatters@hawaii.edu
*E-mail address*: gpicot@hawaii.edu
*E-mail address*: mgranvik@iki.fi
*E-mail address*: jedicke@ifa.hawaii.edu
*E-mail address*: jeremie.vaubaillon@obspm.fr